JAEA-Review
2016-007
DOI:10.11484/jaea-review-2016-007

Boron Release Kinetics from Mixed Melts of Boron Carbide, Stainless Steel and Zircaloy
- A Literature Review on the Behavior of Control Rod Materials under Severe Accidents -

Fidelma Giulia DI LEMMA, Shuhei MIWA and Masahiko OSAKA

LWR Key Technology Development Division
Nuclear Science and Engineering Center
Sector of Nuclear Science Research

March 2016

Japan Atomic Energy Agency
日本原子力研究開発機構

JAEA-Review

国立研究開発法人日本原子力研究開発機構　研究連携成果展開部　研究成果管理課
〒319-1195 茨城県那珂郡東海村大字白方 2 番地4
電話 029-282-6387, Fax 029-282-5920, E-mail:ird-support@jaea.go.jp

Institutional Repository Section,
Intellectual Resources Management and R&D Collaboration Department,
Japan Atomic Energy Agency.
2-4 Shirakata, Tokai-mura, Naka-gun, Ibaraki-ken 319-1195 Japan
Tel +81-29-282-6387, Fax +81-29-282-5920, E-mail:ird-support@jaea.go.jp

JAEA-Review 2016-007

Boron Release Kinetics from Mixed Melts of Boron Carbide, Stainless Steel and Zircaloy

- A Literature Review on the Behavior of Control Rod Materials under Severe Accidents -

Fidelma Giulia DI LEMMA※1, Shuhei MIWA and Masahiko OSAKA

LWR Key Technology Development Division, Nuclear Science and Engineering Center,
Sector of Nuclear Science Research
Japan Atomic Energy Agency
Tokai-mura, Naka-gun, Ibaraki-ken

(Received February 18, 2016)

During a Boiling Water Reactor (BWR) severe accident (SA), complex boron-containing melts can be formed. These melts can be formed due to the interaction of the control rods with the cladding and structural materials, and will contain boron carbide (B_4C), stainless steel (SS) and zircaloy (Zry). Thus they are also known as B_4C/SS/Zry melts. The formation of these melts can affect strongly the boron (B) release kinetics and consequently the fission product (FP) behavior. This review will describe the results of previous studies on B_4C/SS/Zry melts, which will finally provide guidance for the research needs of future experiments. This review shows that reliable set of data and model on the behavior of B_4C under SA conditions exist. On the other hand, those for B_4C/SS/Zry melts are limited, especially regarding their oxidation behavior and B release kinetics. The models applied in current SA codes describe indeed only the B_4C behavior, and have been unsuccessful in simulating core degradation in real and simulated SAs. The improvement of the database for B_4C/SS/Zry melts is thus needed. Based on these conditions, our experimental plan aims to provide thermodynamic and kinetic models for such melts. The final aim is a deep understanding of boron effects on FP behavior and the improvement of its modelling in SA codes.

Keywords: Severe Accident, Boron Carbide, Fission Products, Release Kinetics, B_4C Bearing Melts

---

※1 Post-Doctoral Fellow

炭化ホウ素、ステンレス鋼及びジルカロイの溶融体からのホウ素放出速度
―シビアアクシデント時の制御材炭化ホウ素挙動に係る文献調査―

日本原子力研究開発機構　原子力科学研究部門
原子力基礎工学研究センター　軽水炉基盤技術開発ディビジョン
Fidelma Giulia DI LEMMA※1、三輪　周平、逢坂　正彦

(2016 年 2 月 18 日　受理)

原子炉のシビアアクシデント（SA）時の炉心において、制御材と被覆材の相互作用によりホウ素（B）を含む炭化ホウ素-ステンレス鋼-ジルカロイ（B_4C/SS/Zry）溶融体が形成され得る。この溶融体形成によりホウ素の放出速度は大きな影響を受け、核分裂生成物（FP）挙動にも影響を与える。そこで、B_4C/SS/Zry 溶融体に関する既往研究をレビューして課題を抽出し、課題解決に必要な研究内容を策定した。レビュー結果より、SA 時における B_4C のみの挙動については信頼性の高い実験データや物理モデルが開発されてきているものの、B_4C/SS/Zry 溶融体挙動に係る知見、特に酸化挙動と B 放出速度に関するものは限定的であることがわかった。現在、SA 解析コードで使用されている物理モデルは、B_4C のみの挙動に係る知見に基づくものであり、SA 時や SA を模擬した実験において炉心溶融崩落挙動を再現できないことが示されている。このため、B_4C/SS/Zry 溶融体挙動に係るデータベースの改良が必要であり、B_4C/SS/Zry 溶融体挙動に係る熱力学的及び速度論的モデルを改良するための実験研究計画を策定した。これらの結果は、B の FP 挙動に与える影響評価や SA 解析コードにおける B 挙動モデルの改良に反映していく予定である。

原子力科学研究所：〒319-1195 茨城県那珂郡東海村大字白方 2-4
※1 博士研究員

Contents

目　次

Table List

Figure List

1. Introduction

The Fukushima Daiichi Nuclear Power Station (1F NPS) accident and its present situation have shown the needs for the improvements of severe accidents (SAs) analyses and of the severe accident management measures. Concerning the Light Water Reactor (LWR) SA analysis, we plan to perform fundamental studies on fission product (FP) release and transport behaviors. These could help to improve the radioactive source term assessment. Furthermore by improving FP retention and deposition models and analyzing current decommissioning technologies, we aim to provide guidance for the decommissioning of 1F NPS. We focus our study on the FP chemistry, since FP release and transport behaviors are directly or indirectly affected by the FP chemistry [1], and the description of these phenomena presents still large uncertainties. In our research, we address the issues to be solved for the improvement of SA analysis codes as described below:

- Evaluation of effects of boron (B) release and thermal-hydraulic condition on FP chemical behavior;
- Clarification of the cesium (Cs) chemisorption behavior onto structural materials at high temperatures, such as at upper head of reactor pressure vessel;
- Establishment and improvement of database on thermodynamic and physical properties of FP compounds formed within the reactor;
- Development of experimental techniques for the simulation of FP release and transport, and for a direct measurement of FP chemical forms.

Since the 1F NPS accident a renewed attention has been posed on boron carbide (B_4C) control rods. During the accident, it is believed that the core and B_4C control rod materials melted [2] and relocated downward to the lower plenum. Various studies [3-8] have shown that the relocated melt and bare B_4C material will be oxidized in contact with steam, and consequently boron gaseous/vapor species can be released. Such gases/vapor could react with other gases, vapor and/or aerosols in the reactor, affecting the FP behavior [1,9]. As explained in the U.S. Nuclear Regulatory Commission Guide [10], “the behavior of fission product aerosol is especially affected by the non-radioactive aerosol produced in the accident. This non-radioactive aerosol can include control rod materials, alloying agents from the cladding and other structural materials”. Such effect was further supported by the results of PHEBUS FPT tests, which showed that both the materials released from Pressurized Water Reactor (PWR) and Boiling Water Reactor (BWR) control rods can affect FP behavior [11]. For the evaluation of the source term, it is thus important to investigate the behavior of B_4C bearing melts. However, relatively less knowledge has been obtained so far on the effects of B_4C control material on FPs behavior, compared with those of the Ag-In-Cd control materials for PWR. As reported by Adrouger et al. [12], indeed, “the existing B_4C database is not large enough for plant applications, such as the reduction of the uncertainties on corium behavior and source term evaluation in case of a severe accident". For the improvement of such database, we have proposed an experimental plan to achieve a deeper understanding of B_4C bearing melts behavior, and of their effects on FP behavior under SA conditions. This report aims to point out the current limitations and uncertainties on B_4C bearing melts by analyzing the previous experiments and results. Finally we will describe our experimental plan, which has been motivated by the detected limitations and uncertainties.

2. Literature Review

2.1. Accident Progression

B_4C is widely used as a neutron absorbing control material in BWRs. In a hypothetical SA, it can react with the surrounding stainless steel (SS) cladding in the early stage of the accident, producing an eutectic melt [5,13-14]. This has a melting temperature (around 1473 K) “far below the melting temperatures of all other components” [5]. Reaction between SS and B_4C occurs already at 1073 K, due to thermodynamic instability, but the solid-solid reaction is slow and the liquid phase only start to appear around 1273 K [15]. This reaction is then followed by rapid liquefaction above 1423 K [15]. The formed B_4C bearing melt will first relocate downward inside the cladding, as observed also for B_4C control rods in PWR reactors [5,13]. Only after the failure of the control rod, oxidation of the melt and remaining bare B_4C can take place due to the contact with steam [16].

Experimental tests in absence of the channel box configuration have shown that these melts can also attack the cladding of the surrounding fuel rods by spreading radially. Thus the fuel rod cladding may fail and initiate early release of fuel and FPs [3]. After the interaction with the fuel rod claddings, the melts could incorporate also zirconium (Zr) from the Zircaloy (Zry) fuel cladding, forming B_4C/SS/Zry melts. This interaction can lower again the melting temperature to the eutectic point of 1923 K (100 K lower with respect to the melting point of the Zircaloy cladding of 2023 K) [13,15]. The results of CORA experiments, in which the degradation of heated simulated fuel rods was monitored by camera, showed that radial spread of B_4C/SS melts (in absence of the channel box configuration) will not proceed beyond the first row of fuel rods. However, high quantity of Zry was found to be dissolved, as the cladding walls were completely destroyed (except for the upper and lower part of the bundle ends) [17].

When the cladding fails finally, the formed B_4C/SS/Zry melt will relocate to the lower part of the vessel, and its oxidation and B vaporization will progress from this new location. Various studies [1,3-4] have shown that the formation of B_4C/SS/Zry melts can affect B vaporization, and FP behavior [1,18-19]. The results of PHEBUS FPT3 experiment [9,18-20], in which core degradation of a simulated PWR reactor (scaled down to 1/5000th) was achieved, showed that B_4C control rods can affect the accident progression by promoting a faster and more extensive bundle degradation compared to Ag-In-Cd control rods [20-21].

From the results of CORA experiments [22-23] and thermodynamic consideration by Hofmann et al. [24], three general temperature regimes for the accident progression were identified. These regimes correspond to different degree of core damage summarized in Figure 1, and identified as:

- Between 1473 and 1673 K, the formation of the liquid phase starts due to the interaction of B_4C with SS. At higher temperatures, other low-temperature eutectic interactions can concurrently occur, such as the one between the Zry of the guide tube and the Inconel spacer grids. This leads to a localized failure of the fuel rods and a possible release of FPs, and finally to the localized core damage [24]. However the formed melt can still be cooled. If the melt is cooled and it solidified, it may create a blockage in the core.
- Between 2073 and 2273 K, the metallic Zry of the fuel rods cladding starts to melt. The melt can chemically dissolve the solid UO_2 fuel and the ZrO_2 layer generated on the cladding. Solidification and melting occur repeatedly and extensive core damage is achieved. In this phase, some core regions become no longer coolable.
- Finally between 2873 and 2923 K also the ceramic material $(U,Zr)O_2$ starts to melt and relocate. This leads to the complete melt-down of all materials and a total destruction of the core.

Concerning the relocation behavior of the formed melt, it has been reported that the core melt can relocate through two different paths in the case of BWR configuration, as observed in the XR2 tests [25]. These tests mimic in composition and in geometry the lower part of BWR core including the fuel assembly and simulated the conditions of core melt down. The mixed melt of the control blade and Zry materials was poured over the assembly following a prescribed sequence. The results of the experiments showed that the melt can relocate similarly to the Three Mile Island core accident progression, in so called “wet conditions” progression when large amount of coolant is available, or in the “alternative continuous drainage pathway”. The first pathway consisted of the melt leading to a blocked core configuration. “The water in the lower core causes relocating molten core materials to freeze, forming a dense crust. Subsequent melt collects upon the crust blockage until a molten pool forms. Later, as the pool growth reaches a boundary of the core, the contents of the molten pool (principally molten ceramic fuel) will be released” and will relocate to the lower part of the vessel [25]. The “alternative continuous drainage pathway” consist of a continuous drainage of materials from the core region to the lower head. In this path the lower melting point materials (control blades and Zircaloy materials) will drain first, and later solid or molten ceramic fuel materials will follow. “These two melt progression pathways lead to important differences in the timing and mode of vessel failure, in addition to differences in the rate, temperature and composition of those materials that are ultimately released into the containment environment” [25].

It can be concluded that core degradation is a complex phenomenon, which is strongly influenced by the accident sequence and by the mitigation techniques applied during the accident. Thus different accident sequences can lead to the formation of different melts [26]. For example, some material relocation processes can be different or avoided if mitigation actions are performed [24]. An interesting approach to such core degradation mitigation has been proposed by Hofmann et al. [24]. It consists of the use of Zry instead of stainless steel as cladding for the control materials. Because the reaction between B_4C and Zry occurs at higher temperature than that between B_4C and SS, and its reaction rate is much lower at low temperatures. Thus the use of Zry instead of stainless steel could mitigate and delay core damage in a SA.

2.2. B_4C Bearing Melt Compositions and Phase Relations

High attention has been devolved in the past on assessing the melt compositions and phase relations for B_4C/iron (Fe), B_4C/SS, and B_4C/SS/Zry systems. Phase diagrams for these systems can be found in the work by Tokunaga et al. [26]. In our work, we are interested in BWR configuration. As an example, a 1000 MW class BWR contains about 1200 kg B_4C and about 17000 kg SS as control rod components in the reactor core [27], leading to a weight ratio of SS/B_4C of ca. 14. However, different compositions have been used to assess phase relations in B_4C melts in the previous studies. Takano et al. [28] used a SS/B_4C mass ratio of 9 in all the mixtures, close to the mass ratio in BWRs control blades. In the COLOSS network experiments [12,29], a ratio of 3.5 for SS/B_4C was chosen to have a compromise between a good simulation for PWR and BWR [7]. Luze et al. [16] used mixture compositions which were representative of PWR reactor configurations. They decided to study only B_4C/SS melts, since the thermodynamic calculations for the oxidation of the B_4C/SS/Zry melts showed that liquid melts containing B and Zr in significant proportions were not expected. This last hypothesis is in contradiction with the results of the experiments performed in IRSN [8] and JAEA [28], which showed the high stability of Zr-B compounds. Table 1 summarizes the samples investigated in the previous experiments and the phases detected by the analyses. The details are described in the following paragraphs.

From thermo-chemical calculations according to the NUCLEA database, Luze et al. [16] observed that the solubility of B and C in SS varied with the temperature from 9 wt% at 1296 K to 19 wt% at 1800 K. Dominguez et al. [3,8] confirmed similar B content in their experiments, i.e. B_4C/SS mixtures had B-contents around 9 wt%, while B_4C/SS/Zry mixtures reached B-contents between 6 and 20 wt% [3,8]. These data were obtained from experiments on the simulated B_4C/Fe, B_4C/SS, B_4C/SS/Zry samples with different B contents [3], and on 60 cm long simulated control rods [8]. The tests performed on the simulated samples [3] showed for the solidified B_4C/SS melts the formations of block shaped and needle-like precipitates of Fe/chromium (Cr) borides with some dissolved carbon $(Fe, Cr)_n(B, C)$ (with n between 1.8 and 2.7). The complex eutectic matrix, on the other hand, mainly consisted of boron-free, (Fe, Cr, Ni) carbides and (Fe, Cr) carbides. The simulated control rods [16] were replica of a PWR 1300 MWe, and consisted of B_4C control rods centered inside a Zry guide tube. These rods experienced degradation in steam up to 2273 K and were analyzed by Electron Prove Micro Analyses (EPMA). The analyses were performed at three different heights of the specimens and at two different radial positions. From these analyses, they concluded that:

- The Zr content in the melts depended on the proximity to the Zry guide tube (24-69 wt%). The metallic melts located close to the cladding presented higher content of Zr.
- The metallic melts located inside the gap show two different compositions, generated from the B_4C/SS and/or from the B_4C/SS/Zry interactions. Their B weight depended on the test temperature (3/9 wt% depending on temperature for B_4C/SS, and around 19/20 wt% for B_4C/SS/Zry).

Steinbruck et al. [5, 30] performed also similar studies on solidified B_4C/SS/Zry melts formed in the QUENCH facility. They performed microscopy analyses and concluded that different phases were present. They found that near the B_4C pellet, a $(Fe,Cr)B/(Fe,Cr,Ni)_2B$ (matrix) mixture was predominant in all specimens. Also ZrC and Zr(C, O) were found in this region. Finally other minor phases were identified, such as NiB, CrC_2, ZrB_2, $Zr(B,C)_x$, and $Zr(B,C,O)_x$. They observed also the composition trends as a function of the temperature. The O and Cr content near the B_4C pellet increased with increase of temperature, and finally B and C near the ZrO_2 scale (in the Zr(O,C) and in SS borides respectively) increased with increase of temperature [30].

Takano et al. [28] studied the phase relations and compositions of melts formed due to interaction of B_4C, SS, Zr, ZrO_2, UO_2 and identified the stable phases. They concluded that:

- For the B_4C/SS system the major area of the cross-section was occupied by the Fe_2B-type boride grains, with the composition $(Fe_{0.75}Cr_{0.17}Ni_{0.08})_2B$ (a.k.a. M_2B). Also Cr enriched phases were observed and determined to be $(Fe_{0.47}Cr_{0.51}Ni_{0.02})B$ (a.k.a. MB). Carbon was also detected in these borides with C/(B + C) atomic fractions reaching 0.15 in the M_2B and 0.3 in the MB.
- Concerning the B_4C/SS/Zr system, they found that ZrB_2, ZrC, and $(Fe,Cr,Ni)_2Zr$ were present. ZrB_2 was observed to be more likely formed, as it is a more stable boride than the ferrous borides in the system. Fine ZrC particles also precipitated in the alloy matrix, consuming all the carbon of B_4C, while in the other phases (ZrB_2 and the $(Fe,Cr,Ni)_2Zr$) carbon was detected only in low concentrations. The average composition of the matrix alloy was determined to be 48Fe-10Cr-9Ni-33Zr,

corresponding to the Fe_2Zr-type intermetallic composition. Finally by annealing the melt under an oxidizing condition (p_{O2} = 0.001 atm, 1773 K), ZrB_2 was oxidized and ferrous borides formed instead.

- For Fe/B_4C/Zr, the most stable phases can be extracted by the thermodynamic assessment of the binary and ternary in Fe-Zr-B-C systems. They indicate Fe_2B as the most stable phases in which boron is contained at 1473 K, followed by FeB for Fe/B_4C and ZrB_2 for Fe/B_4C/Zr.

The further CORA experiments [17] showed a similar composition for the B_4C/SS/Zry melt to those for Takano et al. [28]. Zirconium carbide and boride were detected as the most stable phases, and they finally observed that the formed melt was rich in Zr and poor in B and C.

Regarding the behavior of these melts in the lower head of the reactor, the MASCA experiments [31] are an important reference. They showed that B_4C decomposes on contacting the sub-oxidized corium, generating mainly zirconium oxycarbide (ZrC_xO_y) and ZrB_2. Similarly to other experiments, ZrB_2 was chosen to be the most stable phase in which B was detected. The MASCA project consisted of different scale experiments, aimed to simulate corium formation by melting simulated materials and analyzing the solidified melt. They observed a stratification of B in the corium, and found that the upper zone was enriched in B mainly as ZrB_2. This effect was more pronounced due to the Fe addition. Under this condition, they observed that the amount of metal phase increases, and new phases appear. However, their studies have not been conclusive in determining corium composition and B content.

The studies presented demonstrated again that the composition of B_4C bearing melts can vary, as reported also by Dominguez et al. [8]. The melt can be composed of many different complex phases, and their formation behaviors depend strongly on the melt position and on the accident sequence (such as changes in thermo-hydraulics conditions, cladding rupture point, temperature escalation, possible quench by water injection). However, agreement in the studies was found for the identification of the most stable phases as shown in Table 1.

2.3. Reaction Kinetics and the Reaction Layer

The reaction kinetics for B_4C/SS and B_4C/Zry interactions are well known and can be described by parabolic rate laws [24, 32]. The reaction rates have been calculated by Hofmann et al. [24] from microstructural observations, chemical analyses of the reaction layers, and by performing modelling studies. They determined the reaction rates for the solid state reactions [32], and observed that the B_4C/SS reaction rates are two order of magnitude faster than those of B_4C/Zry reaction. The B_4C/SS reaction rates up to 1473 K (before the appearance of liquid phase) can be described by the equation:

$$x^2/t(cm^2/s) = 8.76 * 10^6\, e^{(-378000/RT)}, \qquad (1)$$

where x is reaction depth and t is time. At higher temperatures, they observed a discontinuity in B_4C/SS reaction rate between 1473 and 1498 K, which was attributed to the formation of the liquid phase at the interface [24].

For B_4C/Zry instead they identified two regimes for the reaction. The one up to 1737 K is described by the equation:

$$x^2/t(cm^2/s) = 4.15 * 10^6\, e^{(-122650/RT)} \qquad (2)$$

and the other between 1737 and 1873 K, which show a steep change related to the onset of liquid phase formation, is described by:

$$x^2/t(cm^2/s) = 7.94 * 10^{33} e^{(-1,438300/RT)} \qquad (3).$$

Veshchunov et al. [33] have developed an analytical model for the description of the B_4C/SS reaction kinetics, in the frame of the theory of mass transfer diffusion through a multi-layered structure. They indicated an extremely high mobility of B atoms in the SS matrix. They claimed that: “This model, based on diffusion equations with real values for diffusion coefficients (calculated from experimental data), can be used (instead of simple kinetic correlations valid for isothermal conditions only) for the adequate description of complex temperature transient processes by severe accident code systems” [33].

With respect to the behavior of B_4C/SS reaction layer at different temperatures, data are available in refs.[13,27,32,34], and show that:

- Below the eutectic temperature (1473 K) two reaction layers can be formed mainly in the SS region. A first thin layer adjacent to B_4C was detected, and had a homogeneous appearance. The chemical analysis showed that the first layer consists of MB and M_2B. The second layer consisted mainly of SS matrix, and contained a considerable amount of M_2B precipitates inside grains and/or on grain boundaries.
- Over the eutectic temperature, liquid phase formation occurs, and a three-layer is formed. Two of the three-layers are similar to the ones observed below eutectic temperature. In the middle of these a re-solidified layer was observed.
- The CORA experiments showed further the development mechanism for the B_4C/SS reaction layer. First B_4C particles are infiltrated by the melt. Then the B_4C decomposes and ferrous borides forms in this reaction layer [17].

The further B_4C/Zry interaction can be described instead as follows [32,35]:

- Between 1073 and 1373 K, one reaction layer is formed, consisting of a mixture of ZrB_2 and ZrC.
- In the temperature range from 1473 to 1773 K two reaction layers were observed. The

first reaction layer was similar to the precedent. The subsequent reaction layer consisted mainly of ZrB_2.

- At 1873 K, the two reaction layers are again observed together with the onset of a localized liquid phase formation, which lead to an abrupt change of the reaction rate.
- Finally at 1923 K, their specimens were completely liquefied although at these temperature Zr-B melt and solid ZrB_2 are shown to coexist in a Zr-B phase diagram. This discrepancy has been related, in ref.[32], to the Zr-ZrB_2 eutectic temperature of 1953 K and also to the liquid phases formed at 1888 K by the pseudo binary Zr-($B_{0.5}C_{0.5}$) presented in their work. Moreover they indicated that tin present in Zry may lead to some changes in the onset of liquid phase formation. A scheme summarizing the reaction layers detected and their composition is shown in Figure 2.

In the frame of the COLOSS program, Steinbruck et al. [30] investigated the kinetics of B_4C/SS liquefaction and demonstrated that the eutectic formation is very rapid and can liquefy high quantity of steel. Hollow SS cylinder specimens with central B_4C pellets were tested in an inert atmosphere in the LAVA furnace. This furnace was an inductive furnace, and heated up to 2573 K by a tungsten susceptor. The specimens were tested with different B_4C contents (5 wt%, 1 wt%, and 0.3 wt%) and held at approximately 1523 K for 1 h. The boron carbide was consumed completely in the 1 h tests. Specimens with 5 wt% and 1 wt% B_4C completely liquefied the SS, whereas only 26% of the specimen B_4C was liquefied with 0.3 wt%. Two additional tests of 1 wt% B_4C were performed with shorter times (~5 minutes) at the same temperature. They confirmed the liquefaction to take place very rapidly. “After five minutes, the boron carbide pellet was almost consumed and roughly half of the steel was liquefied. Even after 1 min at a temperature above 1473 K, a significant amount of steel was molten by the eutectic interaction with B_4C” [16,30]. These results are in agreement with the data of Nagase et al. [27], who found strongly increased reaction kinetics between B_4C and SS in the temperature range between 1473 and 1498 K due to the formation of eutectic liquid phases. Their metallography images finally showed a homogeneous melt production for the specimens with higher B_4C contents, while for the specimen with the lowest B_4C contents (0.3 wt%) the analyses showed a transition state between the eutectic melt and the mixture still containing some solid SS.

2.4. Oxidation Progression

The oxidation and vaporization of B_4C and SS were widely studied [4,12-13,16,24,36-37] and are generally well understood. On the other hand, “The oxidation of B_4C-bearing mixtures is a complicated phenomenon, and the mathematical modeling has large uncertainties” [13]. Qualitative experimental results, such as the one obtained from the BECARRE program [3,16] for B_4C/SS melts and the ones of Steinbruck et al. [5], are discussed in the following paragraphs. However, no quantitative models have been developed for B_4C-bearing melts, and "no quantitative kinetics is applied in current severe accident codes", as reported by Zheng et al. [13]. It is important to study these oxidation mechanisms because B_4C oxidation is highly exothermic [37] and can influence the accident progression. A summary of the oxidation models derived from the studies, including the qualitative observations, is shown in Figure 3.

The oxidation kinetics of B_4C in steam can be described by the equation:

$$dx/dt = K_p/x - K_l \qquad (4)$$

where K_p and K_l are the parabolic and linear rate constants, respectively. This relation is regulated by the formation of liquid B_2O_3 barrier and its evaporation. The liquid layer, which covers the surface, acts as a diffusion barrier for the reaction. Its formation depends on temperature and follows parabolic kinetics (K_p). While the evaporation of the liquid B_2O_3 depends on temperature, $H_2O_{(g)}$ partial pressure and thermo-hydraulic conditions, it follows linear kinetics (K_l) [4]. The value of these parameters (K_p and K_l) can be obtained by fitting to experimental data, such as the one obtained in the TG-Rig tests [36]. Different tests provided the experimental evidence for such models, such as the VERDI experiments [12]. In this last study, samples tested were standard B_4C pellets used in French PWR-1300. The B_4C oxidation was quantified by weighing the pellets at the end of the test. The test consisted in heating the pellets up to 1200-1873 K in Ar/steam flow. Also a mass spectrometer was used in the tests for measuring the gaseous species released (H_2, CO, CO_2, CH_4, and boric acids). These tests indicated a large sensitivity of B_4C oxidation to thermal-hydraulic conditions. These results were then used for the development of the B_4C oxidation model and applied in the ICARE/CATHARE code [12]. Another study, which was useful for the development of this oxidation models, was the BOX rig. This study [12, 37] investigated the oxidation of B_4C pellets with different characteristics (such as geometry, porosity, etc.) and evaluated the kinetics of the B_4C oxidation by the H_2 release rates (1473 - 2073 K). Again they observed that the oxidation is strongly influenced by the thermal-hydraulic boundary conditions at the B_4C/atmosphere interface, such as steam partial pressure and flow rate. The microstructure of the B_4C samples was reported to have limited influence on the oxidation behavior and only on the first phase of oxidation [37]. Further the TG-Rig experiments [37] permitted to study B_4C oxidation kinetics by measuring sample temperature and mass change simultaneously with a thermogravimetric (TG) system in the temperature range up to 1573 K. This enabled a precise analysis of B_4C oxidation mechanisms by monitoring the oxidation rates as the temperature progress. Such studies were performed, not only on B_4C pellets, but also separately on graphite and B_2O_3 samples under different conditions, to obtain deep knowledge on the oxidation mechanisms.

Only in the BECARRE experiments [3,16], the oxidation of more complex systems bearing B_4C was studied. Samples with different composition of B_4C/SS (5, 9, and 10% B_4C) and Fe/B (5-10% B and 6.3% B_4C) were investigated. However, their results provided just a qualitative analysis and not a quantitative description of the oxidation phenomena. The limitation came from the impossibility of measuring correctly the sample weight after the tests. In the experiments they measured also H_2 release and monitored the progression of oxidation by a camera. They also performed microstructural analyses on the surface of the samples [3]. From these results, it was observed that at the beginning of the oxidation, the microstructure presents the same phases observed in the original mixtures. While as oxidation progressed, the quantity of B rich phases diminishes, and that of the Fe rich phase increases. At the final stage the microstructure of the mixtures was mainly composed of the Fe phase, while most of the B was released. During the oxidation, they observed the formation of a protective layer on the surface of the samples. This was a brittle layer of inhomogeneous thickness, formed by two different scales: an internal Cr oxide and an external Fe-Cr-O spinel. On the contrary no stable protective layer was observed on the Fe/B samples. From these experiments they determined two stages for oxidation of the melt:

- Moderate oxidation stage, in which a competition mechanism between the formation and consumption of a B-Cr-Si-O liquid layer above the surface of the melt occurs. Again, similarly to the oxidation of B_4C pellet, the formation of the liquid layer acts as a diffusion barrier for the reaction. Its consumption leads to the formation of volatile boric acids. When most of the B is consumed through this mechanism, Cr oxidation rate increases.
- Irregular oxidation stage, in which Cr_2O_3 grains nucleate in the liquid layer as a slag. This slag strengthens by the increase in solid particles with oxidation time. When the oxide (Cr_2O_3) layer grows, a decrease in the oxidation rate can be observed. This oxide layer grows, moves, spreads and cracks. When crack appears, the oxidation rate increases again and H_2 production is enhanced. This mechanism of growth and rupture of the Cr_2O_3 protective layer leads to an irregular oxidation rates.

Finally, in the BECARRE program, they investigated the influence of different parameters on the oxidation mechanism, such as composition, temperature and thermo-hydraulic conditions [3,16]. These conditions seem to influence the protective oxide layer and thereby the oxidation mechanism. They observed that the liquid layer formed above the sample is less protective at lower temperature than at higher temperature, and hence it allows oxygen to reach the B_4C/SS melt surface. From these observations, however, no quantitative models were developed.

Further integral tests, such as QUENCH07 and QUENCH09 [5], were conducted for studying the oxidation and vaporization of simulated control rod (consisting of B_4C pellets, surrounded by SS cladding, contained inside a Zry guide tube). Again only qualitative results were collected. Indeed neither quantitative data on oxidation rate nor information on the B release was collected. Finally Steinbruck et al. [30] showed that the composition of the formed melt can have a strong influence on the oxidation rate. They observed qualitatively that the maximum oxidation rates of B_4C/SS/Zry melts, although with different compositions, are always more than one order of magnitude higher than those of the individual solid materials. Further they indicate [30] that "After melting, the oxidation rate rises steeply and becomes more unstable, the rates scatter widely as a result of the production of inhomogeneous, unstable oxide scale. This unstable behavior may be caused also by rapid local oxidation associated with spraying and fragmentation of the melt." "Small fragmented melt particles offer a large surface to the steam and are consumed very rapidly". A tendency for lower oxidation rates was observed with increasing amounts of B_4C and Zry in the melts. Such phenomena could be related to the generation of solid phases in the melt. This can lead to an increase in viscosity, impeding convection, and thus melt oxidation. Steinbruck et al. [5] concluded, in opposition to the B_4C/SS melts observations, that the oxidation of the melts is not controlled by a protective oxide scale. This may be finally the main reason for the higher oxidation rates observed for these melts.

2.5. Vaporization and Boron Influence on FPs

While the release of CO_x, H_2, and CH_4 gases from the oxidation of B_4C control rods was widely investigated [5-8], boron release studies are limited and available only for simple B_4C. Even though boron release has been shown to strongly influence the source term assessment by interacting with FPs [5-8]. The previous works [5-8] showed that the behavior of B_4C pellets, B_4C/SS and B_4C/SS/Zr compounds differs significantly. They observed that the eutectic formation can decrease H_2 formation by preventing the B oxidation, and thus its vaporization. The equations governing the vaporization of the "simple" B_4C in steam, reported in ref.[11], are listed below and summarized in Figure 3.

$$B_4C + 7H_2O_{(g)} = 2B_2O_{3(l)} + CO_{(g)} + 7H_{2(g)} \tag{5}$$

$$B_4C + 8H_2O_{(g)} = 2B_2O_{3(l)} + CO_{2(g)} + 7H_{2(g)} \tag{6}$$

$$B_4C + 6H_2O_{(g)} = 2B_2O_{3(l)} + CH_{4(g)} + 4H_{2(g)} \tag{7}$$

$$B_4C + 6H_2O_{(g)} = 2B_2O_{3(l)} + C + 6H_{2(g)} \tag{8}$$

and following for the B_2O_3 liquid layer:

$$B_2O_{3(l)} + H_2O_{(g)} = 2HBO_{2(g)} \tag{9}$$

$$B_2O_{3(l)} + 3H_2O_{(g)} = 2H_3BO_{3(g)} \tag{10}$$

$$B_2O_{3(l)} + H_2O_{(g)} = 2/3(HBO_2)_{3(g)} \tag{11}$$

$$B_2O_{3(l)} = B_2O_{3(g)} \tag{12}$$

$$CH_{4(g)} + H_2O_{(g)} = CO_{(g)} + 3H_{2(g)} \tag{13}$$

$$CH_{4(g)} + 2H_2O_{(g)} = CO_{(g)} + 4H_{2(g)} \tag{14}$$

$$CO_{(g)} + H_2O_{(g)} = CO_{2(g)} + H_{2(g)} \tag{15}$$

As it can be observed from the equations, boron will be mainly released as gaseous boric acids (HBO_2, H_3BO_3), formed from the reaction of B_2O_3 liquid layer with steam. In experiments by Luze et al. [16], boric acid production from B_4C/SS mixture was measured but only qualitatively. An enhancement of the production of orthoboric acid (H_3BO_3) was observed, starting at 1373 K. However, further studies are needed for a quantitative evaluation of B release. Furthermore, as less knowledge is available on the reactions between steam and the complex mixtures bearing Zry (B_4C/SS/Zry), further research on this topic is needed.

The PHEBUS FPT3 test showed that B release can have a significant influence on FP behavior. It was shown that B has an effect on iodine release [2] and can inhibit cesium molybdates (Cs-Mo-O) formation [9]. From this experiment the formation of boron blockage in the cold leg was observed [18-19]. Boron was also found to re-vaporize from these deposits. However, data on B release kinetics and its chemical form were not collected in their studies. Miwa et al. [1] aimed to study B effects on FP behavior by thermochemical equilibrium calculations. They investigated the effect of the formation of Fe-B compounds on Cs and I releases, and showed that the B release kinetics will be changed due to the formation of Fe-B-O-H compounds. In particular they found that the release of B was enhanced above approximately 2273 K under steam atmosphere, with the main vapor species released as $CsBO_2$. On the other hand the formation of $CsBO_2$ was limited under steam-starvation atmosphere. This has been related to the decrease in the release of B, due to the formation of low volatile Fe-B compounds. Under steam-starvation conditions, a smaller formation of gaseous hydrogen iodide (HI) and of a high volatile atomic iodine was following predicted from the calculations. Finally, they [1] concluded that the B release kinetics from Fe-B melts, for which no data are available in literature, can affect FP release strongly. A similar effect of B_4C/SS/Zry melt formation, was observed in the QUENCH tests by Steinbruck [6], seen as a decrease in the release of gaseous species. In their experiments low detection of hydrogen was observed. This was related to the formation of the eutectic melts, which prevented B oxidation. It is thus important for an improvement of the prediction of the source term to investigate experimentally and quantitatively B release kinetics from B_4C complex bearing melts.

2.6. Modeling Efforts

Current codes (MELCOR, MENIS, ICARE, etc.) are not able to simulate completely core degradation progression. This has been related mainly to the lack of a model to evaluate oxidation and vaporization of B_4C bearing melts. Although great effort has been performed for their improvement, the current codes include still only models of B_4C oxidation. No models for B_4C bearing melts such as B_4C/SS/Zry melts are present in the codes, which can affect their reliability [16]. For example MELCOR code was not able to describe the core degradation obtained in the CORA experiments. This has been indeed reported in ref.[21] to be related to an unreliable oxidation model in MELCOR. Also the different codes used to simulate the QUENCH test 07 (SCDAP/RELAP5, ICARE/CATHARE and ATHLET-CD) were unsuccessful. In order to obtain congruent results with the experiments, the boundary conditions were modified. The more reproductive results were obtained with ICARE/CATHARE, which gave correct temperature and H_2 release predictions, before the final cool-down phase in QUENCH test 07 [12]. Adrouger et al. [12] reported again that the impossibility of reproducing the experimental results is related to the lack of adequate oxidation models. While MAAP-4 includes a recent model developed for the B_4C/SS interaction. It considers only the B_4C oxidation kinetics and no models are inserted for the oxidation of B_4C bearing melt. While the basic behavior of B_4C under oxidative conditions is well understood and modeled, further improvement are needed to understand quantitatively the behavior of B_4C bearing melts and to update the SA codes models.

3. Experimental Program

As described by our literature review, limitations exist in the current codes in describing core degradation phenomena. These prevent the achievement of a reliable source term description for SAs. The limitations are partly related to the lack of oxidation model and B release model for complex B_4C bearing melts, as reported by Adrouger et al. [12]. While a reliable set of data and models on the behavior of B_4C under SA conditions are available, the data on B_4C-bearing melts are limited and only qualitative. The improvement of such database is the main scope of our experimental program. With our studies, we aim to provide quantitative experimental data on such parameters (oxidation and boron release description) for B_4C/SS/Zry melts. Finally we want to investigate systematically the influence of B release and its kinetics on FP behavior by performing integral experiments. Our final objective is to help develop models for SA codes, and thus improve the source term assessment.

To achieve such goal, separate effect tests named “B-ReK” (Boron Release Kinetics, shown in Figure 4) will be performed in a combination of high temperature Knudsen cell mass spectrometry and thermogravimetry analysis (TGA). Samples will be heated to high temperatures and the gaseous released species will be detected by mass spectrometer. The TGAs will enable us to monitor sample weight and vaporization kinetics as temperature progress, thus to obtain the precise oxidation rate as functions of temperature and oxygen potential, similarly to the TG-Rig experiments [12,16]. The conditions of the experiments are described in Table 2. We will analyze first the behavior of the stable phases contained in the B_4C bearing melts, as obtained from the previously described literature review (Section 2.2), such as the one related to B_4C/Fe interaction (FeB, Fe_2B), and B_4C/Zry (Zr_2B). Further, more complex phases will be analyzed, as the one generated by B_4C/SS interaction (e.g. $(Fe_{0.75}Cr_{0.1}Ni_{0.08})_2B$, $(Fe_{0.47}Cr_{0.51}Ni_{0.02})B$ [28]). Finally B_4C/SS/Zry melts with the compositions corresponding to actual SAs will be applied. A list of the proposed samples for the B_4C bearing melts is presented in Table 3.

Based on the results of the “B-ReK” studies we will perform semi-integral experiments to investigate the effect of B release on the transport, deposition and chemical form of FPs. Also the influence of B release kinetics from complex melts on FP behavior will be investigated in these tests. The experiments will be performed by using a new set-up, called TEST-BENCH (shown in Figure 4). In this experimental set-up, UO_2-simulated fuel containing FP elements will be vaporized in the simulated SA sequence together with B or B containing melts. Coupon will collect the formed deposits at different position in the thermal gradient tube (TGT). By analyzing such coupons together with the deposits on filters and the solutions from the liquid trap, information on FP chemical forms, transport and deposition behavior will be gained. In the further phase of the experiments, different burn-up simulated fuels (sim-fuel) and simulated fuel debris (sim-debris) could be applied.

In Figure 5, a scheme of the experimental plan is presented, in which the final application of the data for the improvement of models is shown. The separate effect studies will provide a deep insight on the oxidation behavior and B release kinetics for the B_4C bearing melts. These could be finally applied for the development of thermodynamic and kinetic models. The experiments with the TEST-BENCH, on the other hand, will provide data on FP release, transport, and deposition under SA conditions and on the influence of realistic B release. Such studies could finally help reducing the current uncertainties on core degradation progression and finally improve source term descriptions for SAs.

4. Summary

Since the 1F NPS accident, a renewed attention has been posed on B_4C control rod behavior under accidental conditions. The existing studies have shown that B_4C control rods can promote accident progression, in terms of timing and extension of core damage. Moreover B release from B_4C/SS/Zry complex melts can affect the FP behavior (such as their chemical form, transport, and deposition). It is thus important for source term evaluation and dose estimation of a BWR SA to understand B release and its kinetics.

From the presented review it is clear that a reliable set of data on the behavior of B_4C under SA conditions exist. Models for the behavior of B_4C are available and are applied in the codes for the simulation of vaporization, oxidation of B_4C and its reaction with other structural materials. However, these models are found to be insufficient to simulate the more complex phenomena occurring during core degradation in real SAs. Most authors have reported that this could be related to a lack of a models for the oxidation and vaporization of complex B_4C bearing melts. Thus the improvement of complex B_4C bearing melts database is needed.

The experimental plan proposed aims to improve the thermodynamic and kinetic models for FP behavior applied in SA codes, by providing experimental data for complex B_4C bearing melts, such as their oxidation kinetics and B release kinetics. Finally we will also investigate, in the new experimental set-up “TEST-BENCH”, the effect of B release on transport and deposition of FPs.

Acknowledgments

The author would like to thanks Dr. M. Takano, Ms. A. Sudo, Messrs. A. Ito and T. Tobita for their support: the fruitful discussion and technical advices, and the help on the practical experimental development. The author will like to thank, further, Dr. F. Nagase for the interest in such research.

References

[1] S. Miwa, et al., Research Program for the Evaluation of Fission Product and Actinide Release Behaviour, Focusing on Their Chemical Forms, Energy Procedia, vol. 71, 2015, pp. 168-181.

[2] F. Tanabe, Analysis of Core Melt Accident in Fukushima Daiichi-Unit 1 Nuclear Reactor, J. Nucl. Sci. Tech., vol. 48 (8), 2011, pp. 1135-1139.

[3] C. Dominguez, Steam oxidation of boron carbide stainless steel liquid mixtures, J. Nucl. Mater., vol. 427 (1-3), 2012, pp. 140-151.

[4] M. Steinbruck, Oxidation of boron carbide at high temperatures, J. Nucl. Mater., 336 (2-3), 2005, pp. 185-193.

[5] M. Steinbruck, et al, Synopsis and outcome of the QUENCH experimental program, Nucl. Eng. Design, vol. 240 (7), 2010, pp. 1714-1727.

[6] M. Veshchunov, et al., Modelling of B_4C oxidation by steam at high temperatures based on separate-effect tests and its application to the bundle experiment QUENCH-07, Tech. Rep., Forschungzentrum Karlsruhe, FZKA-7118, 2006.

[7] C. Hofmann, et al., Analysis and Comparison of Experimental Data of Bundle Tests QUENCH-07 to QUENCH-09 about B_4C Control Rod Behavior, Tech. Rep., Forschungzentrum Karlsruhe, FZKA-7101, 2006.

[8] C. Dominguez, et al., Degradation in steam of 60 cm long B_4C control rods, J. Nucl. Mater., vol. 451 (1-3), 2014, pp. 111-119.

[9] M. Barrachin, et al., Late phase fuel degradation in the Phebus FP tests, Ann. Nucl. Energy, vol. 61, 2013, pp. 36-53.

[10] L. Soffer, et al., Accident Source terms for Light-Water Nuclear Power Plants Final Report, Tech. Rep., Office of Nuclear Regulatory Research, NUREG-1465, 1995.

[11] P.D.W Bottomley, et al., Special Issue: Phebus FP Final Seminar. Ann. Nucl. Energy, vol. 61, 2013, pp. 1-230.

[12] B. Adroguer, et al., Core loss during a severe accident (COLOSS), Nucl. Eng. Design vol. 221, 2003, pp. 55-76.

[13] X. Zheng, et al., Literature Review on Experiments and Models Associated with Degradation and Oxidation of Boron Carbide Control Material during Severe Accidents, Tech. Rep., JAEA, JAEA-Review2014-016, 2014.

[14] P. Hofmann., et al., Chemical Interactions of Reactor Core Materials Up to Very High

Temperatures, Tech. Rep., Forschungzentrum Karlsruhe, KfK-4485, 1989.

[15] O. de Luze, et al., Early phase fuel degradation in Phebus FP: Initiating phenomena of degradation in fuel bundle tests, Ann. Nucl. Energy, vol. 61, 2013, pp.23-35.

[16] O. de Luze, Degradation and oxidation of B_4C control rod segments at high temperatures. A review and code interpretation of the BECARRE program", Nucl. Eng. Design, vol. 259, 2013, pp. 150-163.

[17] G. Schanz, et al., Information on the evolution of severe LWR fuel element damage obtained in the CORA program, J. Nucl. Mater., vol. 188, 1992, pp.131-145.

[18] T. Haste, et al., Transport and deposition in the Phebus FP circuit, Ann. Nucl. Energy, vol. 61, 2013, pp.102-121.

[19] T. Haste, et al., Study of boron behaviour in the primary circuit of water reactors under severe accident conditions: A comparison of Phebus FPT3 results with other recent integral and separate-effects data, Nucl. Eng. Design, vol. 246, 2012, pp. 147-156.

[20] N. Girault, et al., Insights into iodine behaviour and speciation in the Phebus primary circuit, Ann. Nucl. Energy, vol. 61, 2013, pp. 143-156.

[21] K. Trambauer, et al., In-Vessel Core Degradation Code Validation Matrix Update 1996-1999, Tech. Rep., NEA, NEA/CSNI/R(2000)21, 2000.

[22] L. Ott, et al., Interpretation of the results of the CORA-33 dry core boiling water reactor test", Nucl. Eng. Design, vol. 167 (3), 1997, pp. 287-306.

[23] J. Wang, et al., Comparison of CORA and MELCOR core degradation simulation and the MELCOR oxidation model, Nucl. Eng. Design, vol. 276, 2014, pp. 191-201.

[24] P. Hofmann, Current knowledge on core degradation phenomena, a review, J. Nucl. Mater., vol. 270 (12), 1999, pp. 194-211.

[25] R.O. Gauntt, et al., Final Results of the XR2-1 BWR Metallic Melt Relocation Experiment, Tech. Rep., Sandia National Laboratories, NUREG/CR-6527, 1997.

[26] T. Tokunaga, et al., Thermodynamic Analysis of the Phase Equilibria in the Fe-Zr-B System, Mater. Trans., vol. 49 (11), 2008, pp. 2534-2540.

[27] F. Nagase, et al., Chemical interactions between B_4C and stainless steel at high temperatures, J. Nucl. Matr., vol. 245 (1), 1997, pp. 52-59.

[28] M. Takano, et al., Characterization of solidified melt among materials of UO_2 fuel and B_4C control blade, J. Nucl. Sci. Tech., vol 51 (7 -8), 2014, pp. 859-875.

[29] B. Adroguer, et al., Core loss during a severe accident (COLOSS), Nucl. Eng. Design, vol. 235 (2-4), 2005, pp. 173-189.

[30] M. Steinbruck, et al., Degradation and Oxidation of B_4C control rod segments at high temperatures, Tech. Rep., Forschungzentrum Karlsruhe, FZKA-6980, 2004.

[31] V. Asmolov, et al., Masca Project: Major Activities and Results, MASCA Seminar 2004, Aix en Provence, 2004.

[32] P. Hofmann, et al., Reaction Behaviour of B_4C Absorber Material with Stainless Steel

and Zircaloy in Severe LWR Accidents, Tech. Rep., Forschungzentrum Karlsruhe, FZKA-4958, 1989.

[33] M. Veshchunov, et al., Modelling of the interactions between B_4C and stainless steel at high temperatures, J. Nucl. Mater., vol. 226 (12), 1995, pp. 72-91.

[34] I. Campos-Silva, et al., Kinetics of the formation of Fe_2B layers in gray cast iron: Effects of boron concentration and boride incubation time, Appl. Surf. Sci, vol. 255 (229, 2009, pp. 9290-9295.

[35] M. Veshchunov, et al., Modelling of B_4C interactions with Zircaloy at high temperatures, J. Nucl. Mater., vol. 210 (1-2), 1994, pp. 11-20.

[36] W. Krauss, et al., TG-rig tests (thermal balance) on the oxidation of B_4C. Basic experiments, modelling and evaluation approach, Tech. Rep., Forschungzentrum Karlsruhe, FZKA-6883, 2003.

[37] M. Steinbruck, et al., Oxidation of B_4C by steam at high temperatures: New experiments and modelling, Nucl. Eng. Design, vol. 237 (2), 2007, pp.161-181.

Table 1 Summary of the samples tested in the previous studies and the phases detected

Sample	Stable B Phase	Comment	Reference
B_4C/SS	(Fe, Cr)$_n$(B, C) (with n between 1.8 and 2.7)	Matrix boron free	[3]
B_4C/SS/Zry	No phase identification	Boron weight as a function of temperature	[8]
		3/9 wt% for B_4C/SS, 19/20 wt% for SS/B_4C/Zry	
B_4C/SS/Zry QUENCH	(Fe,Cr)B (precipitates), (Fe, Cr, Ni)$_2$B (matrix)		[7]
		Minor phases: ZrB_2, NiB, Zr(B, C)$_x$, and Zr(B, C, O)$_x$	
B_4C/Fe Thermodynamic calculations	Fe_2B, FeB		[28]
B_4C/SS Arc melting	$(Fe_{0.75}Cr_{0.17}Ni_{0.08})_2B$, $(Fe_{0.47}Cr_{0.51}Ni_{0.02})B$		[28]
B_4C/SS/Zry Arc melting	ZrB_2	Carbon detected in low concentration, Boron phases precipitate	[28]
B_4C/SS/Zry CORA	ZrB_2	Detected also ZrC, Melt rich in Zr	[17]
Corium MASCA	ZrB_2	Detected also ZrC, Stratification of B concentration	[31]

Table 2 Proposed experimental conditions of the separate effect tests for B_4C bearing melts

Experiments	Samples /No.	O_2 Partial Pressure /MPa	Max Temperature /K
TGA-MS Ar	1-7	0	1673
TGA-MS O_2	1-7	2.1E^{-2}	1673
TGA-MS H_2O	1-7	1E^{-3}	1673
		1E^{-10}	1673
Test Bench	TBD	1E^{-3}	2073
		1E^{-10}	2073

Table 3 Proposed samples to be tested for B_4C bearing melts

Sample N	Type	Comments
	Single metal compound	
1	Fe_2B	Homogeneous sample
2	FeB	Homogeneous sample
3	ZrB_2	Homogeneous sample
	SS compounds	
4	$(Fe_{0.75}Cr_{0.1}Ni_{0.08})_2B$	
5	$(Fe_{0.47}Cr_{0.51}Ni_{0.02})B$	
	Complex system compound[a)]	
6	SS/B_4C	Composition as in reactor
7	SS/B_4C/Zry	Composition as in reactor

[a)] Tests will be performed also with a pre-oxidized layer.

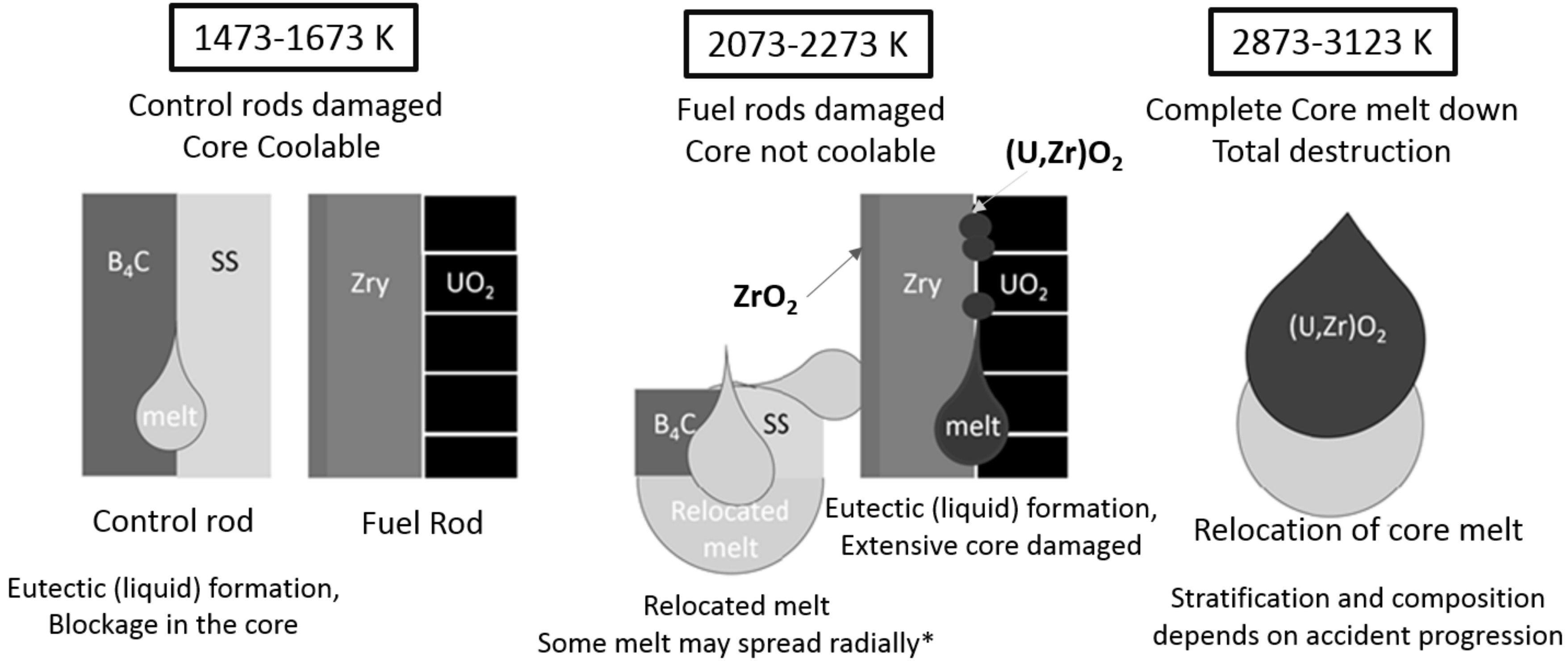

Figure 1 Accident reaction temperature regimes and degree of core damage in the different stages for B_4C including system, as described in ref.[24]

*Some melt may spread radially and attack fuel rods in a PWR configuration (lack of channel box configuration).

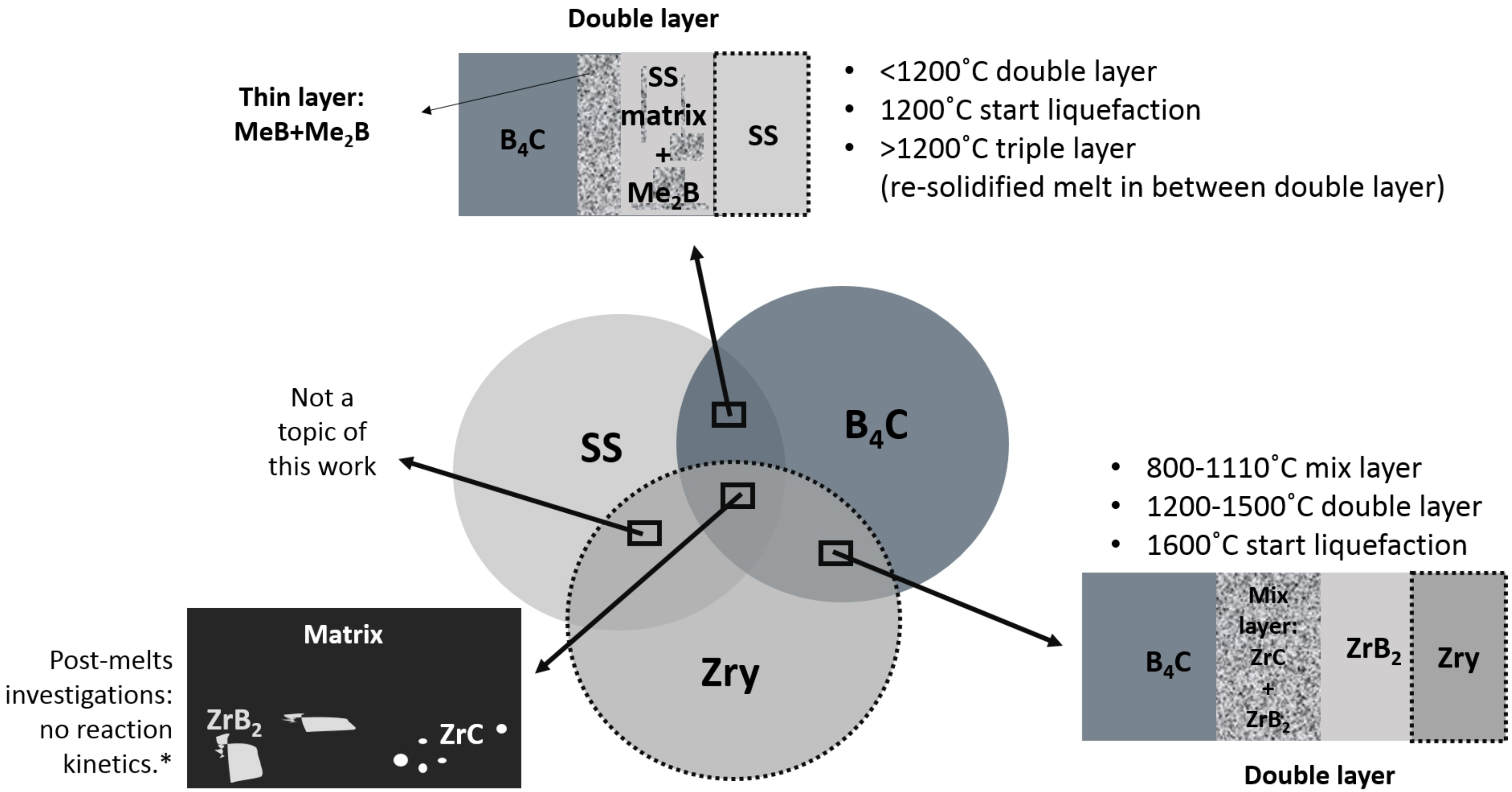

Figure 2 Summary of the reaction layer detected and of the samples compositions for B_4C including system

*Ferrous borides also forms if the initial mixing ratio is rich in SS and B_4C.

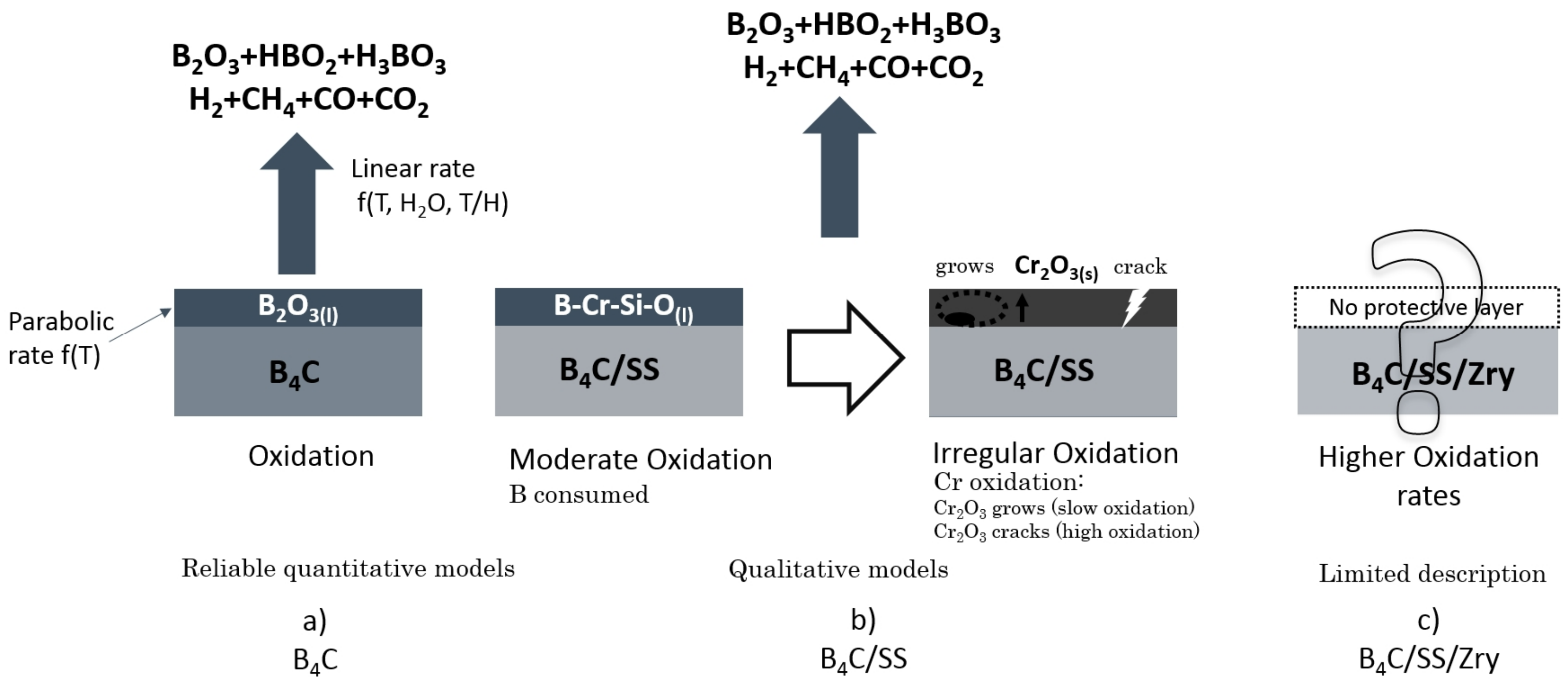

Figure 3 Scheme of the oxidation and vaporization behavior in steam for a) B_4C pellets, b) B_4C/SS mixtures and c) B_4C/SS/Zry

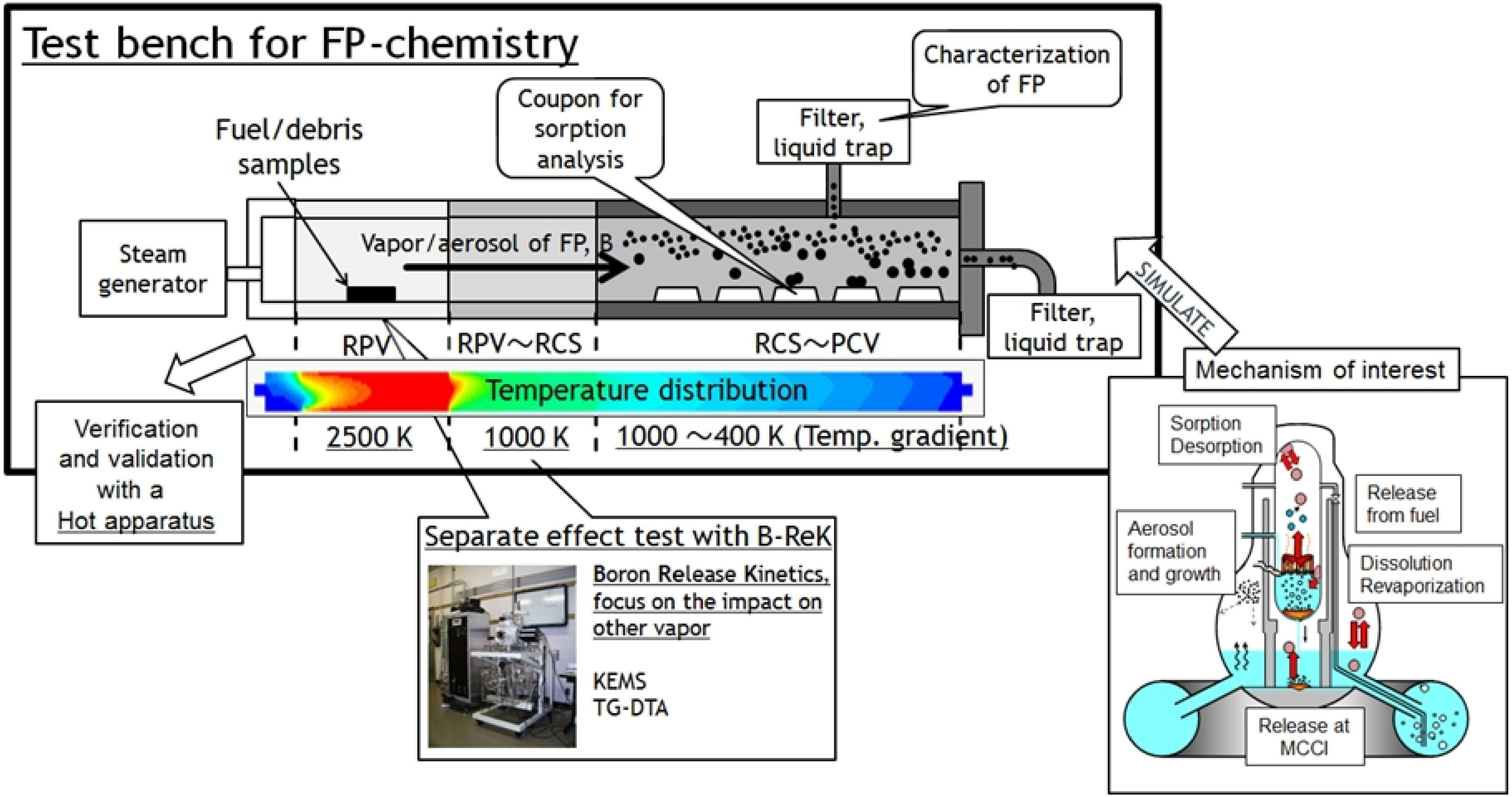

Figure 4 Scheme of the instrumentation applied for the study of boron behavior by separate effect test in the B-ReK, and by semi-integral tests with the TEST-BENCH facility for the analysis of boron influence on FPs transport, deposition and chemistry

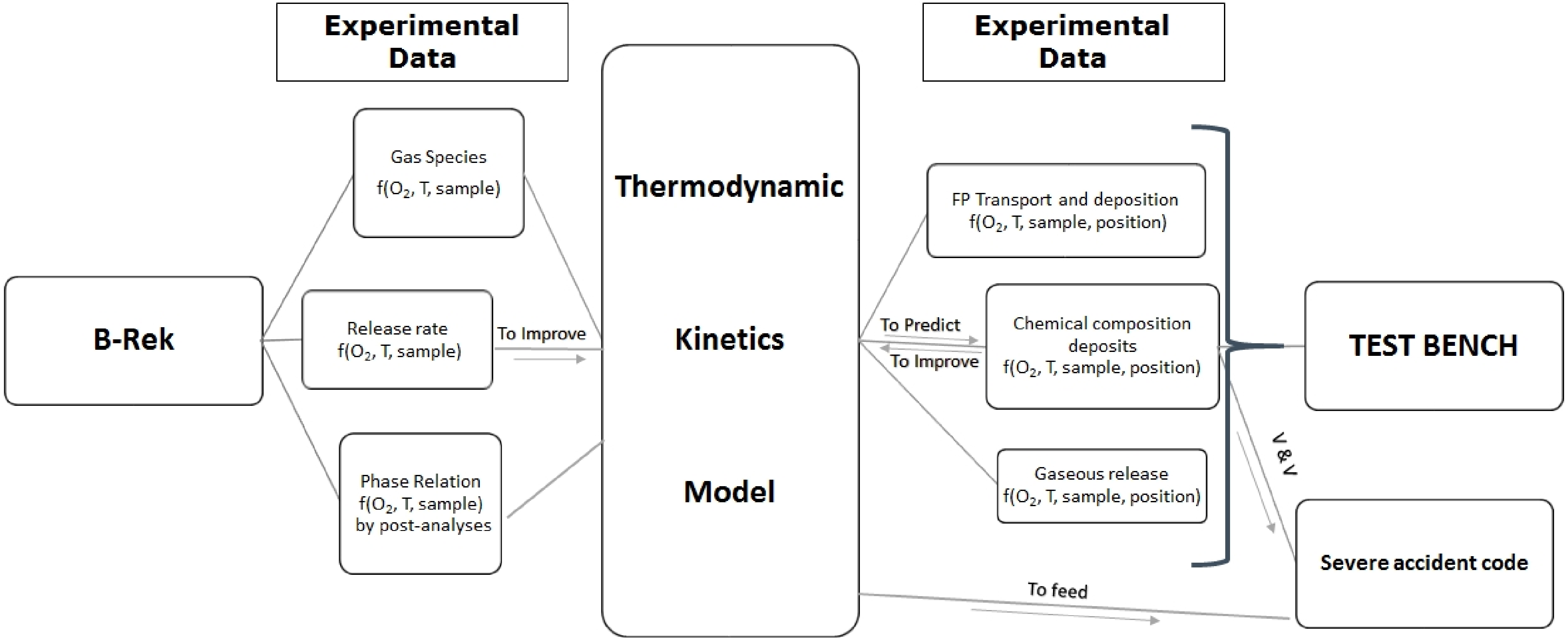

Figure 5 Scheme of the experimental plans and of its application for models development for our studies on boron release kinetics

This is a blank page.

国際単位系（SI）

表１．SI 基本単位

基本量	SI 基本単位	
	名称	記号
長さ	メートル	m
質量	キログラム	kg
時間	秒	s
電流	アンペア	A
熱力学温度	ケルビン	K
物質量	モル	mol
光度	カンデラ	cd

表２．基本単位を用いて表されるSI組立単位の例

組立量	SI 組立単位	
	名称	記号
面積	平方メートル	m^{2}
体積	立方メートル	m^{3}
速さ，速度	メートル毎秒	m/s
加速度	メートル毎秒毎秒	m/s^{2}
波数	毎メートル	m^{-1}
密度，質量密度	キログラム毎立方メートル	kg/m^{3}
面積密度	キログラム毎平方メートル	kg/m^{2}
比体積	立方メートル毎キログラム	m^{3}/kg
電流密度	アンペア毎平方メートル	A/m^{2}
磁界の強さ	アンペア毎メートル	A/m
量濃度(a)，濃度	モル毎立方メートル	mol/m^{3}
質量濃度	キログラム毎立方メートル	kg/m^{3}
輝度	カンデラ毎平方メートル	cd/m^{2}
屈折率(b)	（数字の）　1	1
比透磁率(b)	（数字の）　1	1

(a)　量濃度（amount concentration）は臨床化学の分野では物質濃度（substance concentration）ともよばれる。

(b)　これらは無次元量あるいは次元１をもつ量であるが、そのことを表す単位記号である数字の１は通常は表記しない。

表３．固有の名称と記号で表されるSI組立単位

組立量	SI 組立単位			
	名称	記号	他のSI単位による表し方	SI基本単位による表し方
平面角	ラジアン(b)	rad	1 (b)	m/m
立体角	ステラジアン(b)	sr(c)	1 (b)	m^{2}/m^{2}
周波数	ヘルツ(d)	Hz		s^{-1}
力	ニュートン	N		m kg s^{-2}
圧力，応力	パスカル	Pa	N/m^{2}	m^{-1} kg s^{-2}
エネルギー，仕事，熱量	ジュール	J	N m	m^{2} kg s^{-2}
仕事率，工率，放射束	ワット	W	J/s	m^{2} kg s^{-3}
電荷，電気量	クーロン	C		s A
電位差（電圧），起電力	ボルト	V	W/A	m^{2} kg s^{-3} A^{-1}
静電容量	ファラド	F	C/V	m^{-2} kg^{-1} s^{4} A^{2}
電気抵抗	オーム	Ω	V/A	m^{2} kg s^{-3} A^{-2}
コンダクタンス	ジーメンス	S	A/V	m^{-2} kg^{-1} s^{3} A^{2}
磁束	ウエーバ	Wb	Vs	m^{2} kg s^{-2} A^{-1}
磁束密度	テスラ	T	Wb/m^{2}	kg s^{-2} A^{-1}
インダクタンス	ヘンリー	H	Wb/A	m^{2} kg s^{-2} A^{-2}
セルシウス温度	セルシウス度(e)	℃		K
光束	ルーメン	lm	cd sr(c)	cd
照度	ルクス	lx	lm/m^{2}	m^{-2} cd
放射性核種の放射能(f)	ベクレル(d)	Bq		s^{-1}
吸収線量, 比エネルギー分与, カーマ	グレイ	Gy	J/kg	m^{2} s^{-2}
線量当量, 周辺線量当量, 方向性線量当量, 個人線量当量	シーベルト(g)	Sv	J/kg	m^{2} s^{-2}
酸素活性	カタール	kat		s^{-1} mol

(a)SI接頭語は固有の名称と記号を持つ組立単位と組み合わせても使用できる。しかし接頭語を付した単位はもはやコヒーレントではない。

(b)ラジアンとステラジアンは数字の１に対する単位の特別な名称で、量についての情報をつたえるために使われる。実際には、使用する時には記号rad及びsrが用いられるが、習慣として組立単位としての記号である数字の１は明示されない。

(c)測光学ではステラジアンという名称と記号srを単位の表し方の中に、そのまま維持している。

(d)ヘルツは周期現象についてのみ、ベクレルは放射性核種の統計的過程についてのみ使用される。

(e)セルシウス度はケルビンの特別な名称で、セルシウス温度を表すために使用される。セルシウス度とケルビンの単位の大きさは同一である。したがって、温度差や温度間隔を表す数値はどちらの単位で表しても同じである。

(f)放射性核種の放射能（activity referred to a radionuclide）は、しばしば誤った用語で”radioactivity”と記される。

(g)単位シーベルト（PV,2002,70,205）についてはCIPM勧告2（CI-2002）を参照。

表４．単位の中に固有の名称と記号を含むSI組立単位の例

組立量	SI 組立単位		
	名称	記号	SI 基本単位による表し方
粘度	パスカル秒	Pa s	m^{-1} kg s^{-1}
力のモーメント	ニュートンメートル	N m	m^{2} kg s^{-2}
表面張力	ニュートン毎メートル	N/m	kg s^{-2}
角速度	ラジアン毎秒	rad/s	m m^{-1} s^{-1}=s^{-1}
角加速度	ラジアン毎秒毎秒	rad/s^{2}	m m^{-1} s^{-2}=s^{-2}
熱流密度，放射照度	ワット毎平方メートル	W/m^{2}	kg s^{-3}
熱容量，エントロピー	ジュール毎ケルビン	J/K	m^{2} kg s^{-2} K^{-1}
比熱容量，比エントロピー	ジュール毎キログラム毎ケルビン	J/(kg K)	m^{2} s^{-2} K^{-1}
比エネルギー	ジュール毎キログラム	J/kg	m^{2} s^{-2}
熱伝導率	ワット毎メートル毎ケルビン	W/(m K)	m kg s^{-3} K^{-1}
体積エネルギー	ジュール毎立方メートル	J/m^{3}	m^{-1} kg s^{-2}
電界の強さ	ボルト毎メートル	V/m	m kg s^{-3} A^{-1}
電荷密度	クーロン毎立方メートル	C/m^{3}	m^{-3} s A
表面電荷	クーロン毎平方メートル	C/m^{2}	m^{-2} s A
電束密度，電気変位	クーロン毎平方メートル	C/m^{2}	m^{-2} s A
誘電率	ファラド毎メートル	F/m	m^{-3} kg^{-1} s^{4} A^{2}
透磁率	ヘンリー毎メートル	H/m	m kg s^{-2} A^{-2}
モルエネルギー	ジュール毎モル	J/mol	m^{2} kg s^{-2} mol^{-1}
モルエントロピー, モル熱容量	ジュール毎モル毎ケルビン	J/(mol K)	m^{2} kg s^{-2} K^{-1} mol^{-1}
照射線量（Ｘ線及びγ線）	クーロン毎キログラム	C/kg	kg^{-1} s A
吸収線量率	グレイ毎秒	Gy/s	m^{2} s^{-3}
放射強度	ワット毎ステラジアン	W/sr	m^{4} m^{-2} kg s^{-3}=m^{2} kg s^{-3}
放射輝度	ワット毎平方メートル毎ステラジアン	W/(m^{2} sr)	m^{2} m^{-2} kg s^{-3}=kg s^{-3}
酵素活性濃度	カタール毎立方メートル	kat/m^{3}	m^{-3} s^{-1} mol

表５．SI 接頭語

乗数	名称	記号	乗数	名称	記号
10^{24}	ヨタ	Y	10^{-1}	デシ	d
10^{21}	ゼタ	Z	10^{-2}	センチ	c
10^{18}	エクサ	E	10^{-3}	ミリ	m
10^{15}	ペタ	P	10^{-6}	マイクロ	µ
10^{12}	テラ	T	10^{-9}	ナノ	n
10^{9}	ギガ	G	10^{-12}	ピコ	p
10^{6}	メガ	M	10^{-15}	フェムト	f
10^{3}	キロ	k	10^{-18}	アト	a
10^{2}	ヘクト	h	10^{-21}	ゼプト	z
10^{1}	デカ	da	10^{-24}	ヨクト	y

表６．SIに属さないが、SIと併用される単位

名称	記号	SI 単位による値
分	min	1 min=60 s
時	h	1 h =60 min=3600 s
日	d	1 d=24 h=86 400 s
度	°	1°=(π/180) rad
分	’	1’=(1/60)°=(π/10 800) rad
秒	”	1”=(1/60)’=(π/648 000) rad
ヘクタール	ha	1 ha=1 hm^{2}=10^{4}m^{2}
リットル	L，l	1 L=1 l=1 dm^{3}=10^{3}cm^{3}=10^{-3}m^{3}
トン	t	1 t=10^{3} kg

表７．SIに属さないが、SIと併用される単位で、SI単位で表される数値が実験的に得られるもの

名称	記号	SI 単位で表される数値
電子ボルト	eV	1 eV=1.602 176 53(14)×10^{-19}J
ダルトン	Da	1 Da=1.660 538 86(28)×10^{-27}kg
統一原子質量単位	u	1 u=1 Da
天文単位	ua	1 ua=1.495 978 706 91(6)×10^{11}m

表８．SIに属さないが、SIと併用されるその他の単位

名称	記号	SI 単位で表される数値
バール	bar	1 bar=0.1MPa=100 kPa=10^{5}Pa
水銀柱ミリメートル	mmHg	1 mmHg≈133.322Pa
オングストローム	Å	1 Å=0.1nm=100pm=10^{-10}m
海里	M	1 M=1852m
バーン	b	1 b=100fm^{2}=(10^{-12}cm)^{2}=10^{-28}m^{2}
ノット	kn	1 kn=(1852/3600)m/s
ネーパ	Np	SI単位との数値的な関係は、対数量の定義に依存。
ベル	B	
デシベル	dB	

表９．固有の名称をもつCGS組立単位

名称	記号	SI 単位で表される数値
エルグ	erg	1 erg=10^{-7} J
ダイン	dyn	1 dyn=10^{-5}N
ポアズ	P	1 P=1 dyn s cm^{-2}=0.1Pa s
ストークス	St	1 St =1cm^{2} s^{-1}=10^{-4}m^{2} s^{-1}
スチルブ	sb	1 sb =1cd cm^{-2}=10^{4}cd m^{-2}
フォト	ph	1 ph=1cd sr cm^{-2} =10^{4}lx
ガル	Gal	1 Gal =1cm s^{-2}=10^{-2}ms^{-2}
マクスウエル	Mx	1 Mx = 1G cm^{2}=10^{-8}Wb
ガウス	G	1 G =1Mx cm^{-2} =10^{-4}T
エルステッド(a)	Oe	1 Oe ≙ (10^{3}/4π)A m^{-1}

(a)　３元系のCGS単位系とSIでは直接比較できないため、等号「 ≙ 」は対応関係を示すものである。

表10．SIに属さないその他の単位の例

名称	記号	SI 単位で表される数値
キュリー	Ci	1 Ci=3.7×10^{10}Bq
レントゲン	R	1 R = 2.58×10^{-4}C/kg
ラド	rad	1 rad=1cGy=10^{-2}Gy
レム	rem	1 rem=1 cSv=10^{-2}Sv
ガンマ	γ	1 γ =1 nT=10^{-9}T
フェルミ		1 フェルミ=1 fm=10^{-15}m
メートル系カラット		1 メートル系カラット= 0.2 g = 2×10^{-4}kg
トル	Torr	1 Torr = (101 325/760) Pa
標準大気圧	atm	1 atm = 101 325 Pa
カロリー	cal	1 cal=4.1858J（「15℃」カロリー），4.1868J（「IT」カロリー），4.184J（「熱化学」カロリー）
ミクロン	µ	1 µ =1µm=10^{-6}m

（第8版，2006年）